THE JOURNAL OF BIOLOGICAL CHEMISTRY VOL. 285, NO. 3, pp. 1950–1956, January 15, 2010

Unraveling of the E-helices and Disruption of 4-Fold Pores Are Associated with Iron Mishandling in a Mutant Ferritin Causing Neurodegeneration*

Received for publication, July 9, 2009, and in revised form, November 17, 2009 Published, JBC Papers in Press, November 18, 2009, DOI 10.1074/jbc.M109.042986

Martin A. Baraibar[‡1], **Barry B. Muhoberac**[§1,2], **Holly J. Garringer**[‡], **Thomas D. Hurley**[¶], **and Ruben Vidal**[‡3]

From the [‡]*Departments of Pathology and Laboratory Medicine and* [¶]*Biochemistry and Molecular Biology, Indiana University School of Medicine and the* [§]*Department of Chemistry and Chemical Biology, Indiana University-Purdue University Indianapolis, Indianapolis, Indiana 46202*

Mutations in the coding sequence of the ferritin light chain (FTL) gene cause a neurodegenerative disease known as neuroferritinopathy or hereditary ferritinopathy, which is characterized by the presence of intracellular inclusion bodies containing the mutant FTL polypeptide and by abnormal accumulation of iron in the brain. Here, we describe the x-ray crystallographic structure and report functional studies of ferritin homopolymers formed from the mutant FTL polypeptide p.Phe167SerfsX26, which has a C terminus that is altered in amino acid sequence and length. The structure was determined and refined to 2.85 Å resolution and was very similar to the wild type between residues Ile-5 and Arg-154. However, instead of the E-helices normally present in wild type ferritin, the C-terminal sequences of all 24 mutant subunits showed substantial amounts of disorder, leading to multiple C-terminal polypeptide conformations and a large disruption of the normally tiny 4-fold axis pores. Functional studies underscored the importance of the mutant C-terminal sequence in iron-induced precipitation and revealed iron mishandling by soluble mutant FTL homopolymers in that only wild type incorporated iron when in direct competition in solution with mutant ferritin. Even without competition, the amount of iron incorporation over the first few minutes differed severalfold. Our data suggest that disruption at the 4-fold pores may lead to direct iron mishandling through attenuated iron incorporation by the soluble form of mutant ferritin and that the disordered C-terminal polypeptides may play a major role in iron-induced precipitation and formation of ferritin inclusion bodies in hereditary ferritinopathy.

In humans, nucleotide insertions in the coding sequence of the ferritin light chain (FTL)[4] gene (1–6) are associated with an autosomal dominant neurodegenerative disease named neuroferritinopathy (1) or hereditary ferritinopathy (HF) (2, 7). Clinically, HF is characterized by an abnormal involuntary movement disorder and cognitive decline. Neuropathologically, the disease is characterized by the presence of intracellular ferritin inclusion bodies and iron accumulation principally in the central nervous system (8). With one exception (9), all reported HF causing mutations are insertions in exon 4 of the FTL gene (1–6) that cause a frameshift leading to FTL polypeptides of increased length and altered C-terminal sequence.

In mammals, ferritin is the main intracellular iron storage protein and plays an essential role in iron homeostasis as well as detoxification (10). Different organ systems fine-tune ferritin function by producing heteropolymers composed of different ratios of light (FTL) and heavy chain (FTH1) polypeptides (10–12), which are ~50% identical in amino acid sequence and of similar length. Ferritin heteropolymers are formed from the self- assembly of FTL and FTH1 subunits into 24-mer spherical shells ranging from 450 to 500 kDa in mass with an external diameter of 12 nm and an internal nanocavity of 8 nm. The latter is the storage location of up to 4,500 iron atoms as a hydrated ferric oxide mineral core (13, 14), which results from a combination of protein-based oxidation and inorganic aqueous iron chemistry. Thus, highly insoluble ferric iron can be stored and prevented from interacting with other proteins and peptides, as well as from undergoing uncontrolled redox reactions.

FTL and FTH1 subunits consist of a bundle of four parallel α-helices (A–D), a long extended loop (connecting helices B and C), and a C terminus with a short α-helix (E), which is involved in important stabilizing interactions around the 4-fold symmetry axes (11, 15, 16). Although both subunit types share a high degree of conformational similarity, they have diverse functional roles due to particular amino acid sequence differences; FTL enhances iron nucleation and protein stability, whereas FTH1 performs ferroxidase activity, which causes the oxidation of ferrous iron as the first step in the iron nucleation and mineralization processes (11). Interestingly, homopoly-

* This work was supported, in whole or in part, by National Institutes of Health Grants NS050227 and NS050227-04S1. Results shown in this study are derived from work performed at Argonne National Laboratory, Structural Biology Center at the Advanced Photon Source.

The atomic coordinates and structure factors (codes 3HX2, 3HX5, and 3HX7) have been deposited in the Protein Data Bank, Research Collaboratory for Structural Bioinformatics, Rutgers University, New Brunswick, NJ (http://www.rcsb.org/).

[1] Both authors contributed equally to this work.

[2] To whom correspondence may be addressed: Dept. of Chemistry and Chemical Biology, Indiana University-Purdue University Indianapolis, 402 N Blackford St. LD 326, Indianapolis, IN 46202. Tel.: 317-274-6885; Fax: 317-274-4701; E-mail: bmuhober@iupui.edu.

[3] To whom correspondence may be addressed: Dept. of Pathology and Laboratory Medicine, Indiana University School of Medicine, 635 Barnhill Dr. MSB A136, Indianapolis, IN 46202. Tel.: 317-274-1729; Fax: 317-278-6613; E-mail: rvidal@iupui.edu.

[4] The abbreviations used are: FTL, ferritin light chain; HF, hereditary ferritinopathy; FTH1, ferritin heavy chain; WT-FTL, wild type ferritin light chain; MT-FTL, mutant (p.Phe167SerfsX26) ferritin light chain; TRUN-FTL, C-terminally truncated FTL polypeptide (p.S167X); MES, 2-(*N*-morpholino)ethanesulfonic acid.

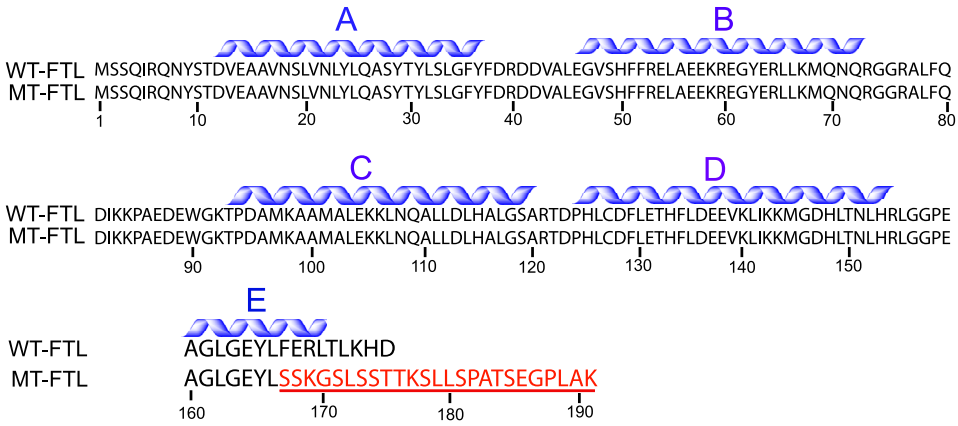

FIGURE 1. **Sequence alignment of WT- and MT-FTL (p.Phe167SerfsX26) polypeptides.** The five α-helical domains (*A–E*) of the WT-FTL subunit are shown *above* their respective sequences (Protein Data Bank code 2fg4). The MT-FTL polypeptide has a C terminus that is altered in sequence and length starting at residue Phe-167. The truncated FTL polypeptide p.S167X (TRUN-FTL) has a sequence identical to the WT-FTL polypeptide until it terminates at Leu-166 (amino acids 1–166).

mers composed of FTL subunits alone have iron incorporation ability, although at a substantially reduced rate from heteropolymers containing both FTL and FTH1 subunits (11). The subunits are structurally related by 4-, 3-, and 2-fold symmetry axes (4-3-2 symmetry) and pack tightly together except at the 3- and 4-fold axes where there are narrow pores traversing the shell. Residues around the eight 3-fold pores are predominantly hydrophilic and have been proposed as the main entry route for iron and the sites for ferrous iron oxidation (11). However, the six 4-fold pores are mainly hydrophobic and smaller; it has been suggested that they provide an exit pathway for protons during iron mineralization (17).

We previously presented spectroscopic and biochemical studies of recombinant mutant FTL homopolymers (24-mer) assembled from the p.Phe167SerfsX26 polypeptide (Fig. 1), which has 9 substitutions and a 16-amino acid extension on its C terminus (18). Here, we present the x-ray crystallographic structure of homopolymers of the mutant FTL polypeptide at 2.85 Å resolution, as well as further functional studies.

EXPERIMENTAL PROCEDURES

Cloning, Expression, and Purification of Recombinant Ferritins—Human wild type (WT-FTL) and the p.Phe167SerfsX26 mutant (MT-FTL) ferritin light chain polypeptides were expressed and purified as homopolymers (24-mer) as described previously (18). A stop codon was introduced in codon 167 (Ser) by PCR to generate the p.S167X, a C-terminally truncated FTL polypeptide (TRUN-FTL). PCR amplification of a human FTL cDNA was performed using the upstream primer F1 5′-TGG ATC CAT CGA AGG TCG TAT GAG CTC CCA GAT T-3′ and the downstream primer R2 5′-TTG ATG TCT CGA GTT AGA GAT ACT CGC C-3′. The cDNA was introduced into the pET-28a(+) expression vector (Novagen, EMD Chemicals Inc.) between the BamHI and XhoI sites, downstream from and in-frame with the sequence encoding an N-terminal His_6 tag. To eliminate the His_6 tag (included in the expression vector), the sequence of the vector was modified by introducing the recognition sequence for cleavage by Factor Xa (GE Healthcare) before the coding sequence of the FTL gene. The construct was confirmed by DNA sequencing in both directions and transformed into BL21 (DE3) *Escherichia coli* (Invitrogen). Expression and purification of the truncated homopolymers followed the same procedure described previously (18). Protein concentration was determined using the BCA reagent (Pierce) with bovine serum albumin as standard. For iron removal (apoferritin production), recombinant ferritin homopolymers were incubated with 1% thioglycollic acid, pH 5.5, and 2,2′-bipyridine, followed by dialysis against 0.1 M phosphate buffer, pH 7.4, as described previously (19). After this procedure, less than five atoms of iron per ferritin 24-mer were consistently achieved, as determined by the colorimetric ferrozine-based assay for the quantification of iron (20).

Crystallization and Structure Determination of Homopolymers of Mutant Ferritin—Crystals of MT-FTL homopolymers were grown from apoprotein solutions concentrated to 4.5 mg/ml in 0.1 M MES buffer, pH 6.5, and equilibrated with solutions containing the same buffer with 5% of polyethylene glycol 6000 (w/v) and 2% of ethylene glycol (w/v). The crystals grew as large irregular plates, which diffracted weakly on our home x-ray source. The diffraction data were collected at the Structural Biology Center beamline 19-ID located at the Advanced Photon Source within the Argonne National Laboratory to a resolution limit of 2.85 Å. The structure was solved through a combination of automated and manual molecular replacement using wild type human FTL homopolymers (24 subunits) as the search model and the data to 4 Å. The program AMoRe (21) found three independent 24-mers in the triclinic cell without difficulty, but additional solutions were not sufficiently separated from the initial three for automated placement. This partial model for the asymmetric unit was used to calculate σ_A-weighted $2F_o - F_c$ electron density maps and an additional three 24-mers were located through direct inspection and manual docking into the resulting electron density in regions where sufficient volume was available through crystal packing analyses. Consequently, six independent copies of the 24-mer composed the asymmetric unit. After inspection of the initial electron density maps indicated disordering or large structural shifts from residue 154 onward, all subunits were truncated at residue 155 until sufficient $F_o - F_c$ and $2F_o - F_c$ electron density was present to build additional residues into the model. All structural models were refined with the software Crystallography and NMR System (CNS) (22) using noncrystallographic symmetry restraints on all atoms with a weight of 25 kcal/mol for the first few rounds of refinement and subsequently only on the main chain atoms with a weight of 10 kcal/mol for residues 6–153 in each subunit during the later rounds of refinement. The size of this structure required modification of the CNS source code to accommodate the 144 noncrystallographic sym-

metry operators and the more than 187,000 non-hydrogen atoms present in the structure. Because of disordering and lack of well defined electron density at the C termini of the 144 chains, 1 chain terminated at Arg-154, 15 at Leu-155, 14 at Gly-156, 2 at Gly-157, 14 at Pro-158, 21 at Glu-159, 38 at Ala-160, 19 at Gly-161, 0 at Leu-162 and Gly-163, 7 at Glu-164, and 13 at Tyr-165. All visualization and rebuilding of the structure were accomplished using the program Coot (23).

Characterization of the Solubility of Apoferritins with Increasing Iron Loading—Following routine iron-loading procedures detailed elsewhere (19, 24, 25), freshly prepared ferrous ammonium sulfate in 10 mM HCl was aerobically mixed with either WT-, MT-, or TRUN-FTL apoferritin homopolymers in 0.1 M Hepes buffer, pH 7.4, to produce final concentrations from 0.5 to 4.0 mM iron and 1 μM homopolymer. The solution was incubated for 2 h at room temperature and then centrifuged at 10,000 $\times$ *g* for 15 min. The supernatants were electrophoresed on nondenaturing 3–8% polyacrylamide gels (Invitrogen) and stained for protein with Coomassie Blue.

Spectrophotometric Characterization of Initial Iron Incorporation into Apoferritins—FTL homopolymers in 0.1 M Hepes buffer, pH 7.0, were aerobically mixed with freshly made ferrous ammonium sulfate to produce final concentrations of 1 mM iron and 1 μM homopolymer. Iron incorporation/hydrolysis was monitored at room temperature by the increase in absorption at 310 nm for the first 550 s after mixing (19, 24, 26). Ferrous ammonium sulfate mixed with buffer alone was used as a control. Samples were run by triplicates in each experiment. Statistical analysis was done using GraphPad Prism version 4.03 (GraphPad Software, San Diego).

Direct Competition between WT- and MT-FTL Apoferritins for Iron Incorporation—Approximately equal molar amounts of WT- and MT-FTL homopolymers were mixed together in 0.1 M Hepes buffer, pH 7.0. This solution was then mixed with ferrous ammonium sulfate (resulting in final concentrations of 0.1 mM iron and 0.1 μM homopolymer) and then incubated aerobically for 30 min at room temperature. After centrifugation at 10,000 $\times$ *g* for 10 min, the supernatants were electrophoresed on nondenaturing gels and stained for protein with Coomassie Blue or for iron incorporation with Prussian blue (26, 27).

RESULTS

Crystallographic Structure of Mutant Homopolymers Exhibited a Large but Localized Change—The structure of human MT-FTL 24-mer apoprotein was solved and refined to 2.85 Å resolution with good overall stereochemistry. Crystallographic statistics are reported in Table 1. MT-FTL subunits assembled into well formed spherical shells (Fig. 2*A*) of dimension and shape very similar to the WT-FTL homopolymers. The 4-helix bundle (helices A–D) was maintained in the mutant with subunit structure very similar to the WT-FTL between residues Ile-5 and Arg-154 (Fig. 2*B*). The subunit dimer interfaces, as well as the dimer-to-dimer contacts, were basically unchanged. Individual subunits aligned with root mean square deviation values of 0.4 Å, and whole 24 subunit arrangements aligned with root mean square values of 0.5 Å for the Cα positions of residues Arg-6 to Leu-152. The only major exception to this overall structural similarity was in the C terminus. The structure of the eight 3-fold pores was similar in the mutant and wild type homopolymers. MT-FTL homopolymers exhibited one bound metal ion, which was tentatively assigned as Ca^{2+}, within each of the eight pores. Although no metal was added during crystallization, the factor Xa digestion buffer used during the removal of the His tag contained 1 mM $CaCl_2$. Each of the three pore-forming subunits donated one Asp-128 and one Glu-131 resulting in a six-coordinate metal site close to the interior surface of the protein. The Cys-127, which can assume two conformations through rotation, was rotated away from its metal binding conformation in the mutant as is found in a subset of the conformations in the WT-FTL (16), and the pore itself was slightly broader in the mutant than the wild type. Although the residues of the metal nucleation site were evident, the assignment of nearby electron density to bound metal *versus* water was unclear and left unassigned.

TABLE 1
X-ray diffraction data and refinement statistics

Data collection	
Space group	P1 (triclinic)
Cell dimensions	a = 212 Å, b = 234 Å, c = 250 Å α = 95°, β = 115°, γ = 115°
Resolution	50.0-2.85 Å
Total observations	1,993,627
Unique reflections	846,572
Completeness	94.2% (62.9%)[a]
$\langle I \rangle / \sigma_{\langle I \rangle}$	9.7 (1.9)[a]
R_{merge}	0.080 (0.32)[a]
Refinement	
R_{free}/R_{work}	0.291/0.249 (0.47/0.42)[a]
Average main chain NCS[b] r.m.s.d.[b] (residues 9–158)	0.25 Å
r.m.s.d. ideal bonds	0.008 Å
r.m.s.d. ideal angles	1.20 Å
Protein atoms in model	184,525
Bound metal ions	48
Bound water molecules	2745

[a] Values in parentheses are for the highest resolution shell (2.95-2.85 Å).
[b] NCS is noncrystallographic symmetry; r.m.s.d. is root mean square deviation.

The N termini and most notably the C termini of the MT-FTL homopolymer subunits differed markedly in structure from the wild type. Importantly, the E-helices, which form the 4-fold pores, were not observed in the electron density map in all subunits of the mutant. In addition, the path of residues from Leu-155 through Tyr-165 differed considerably from that of the wild type when it was observed. For example, in one mutant pore the short loops connecting the ends of the D-helices and the beginning of the E-helices in the wild type were shifted ~90° in the mutant (Fig. 2*C*). Residues Gly-156 to Lys-191 were generally disordered with approximately half of the 144 characterized subunits exhibiting interpretable electron density data up to residue Glu-159. Several subunits only provided interpretable electron density data up to residue Leu-155, although others continued on to Tyr-165. This structural rearrangement can be seen with the wild type C-terminal E-helix (*blue*) and three examples of the visible portions of the C termini from different mutant subunits (Fig. 2*B*). The D-helix remained unchanged in structure and position, even in those subunits in which interpretable electron density data ended at Leu-155, just 1 residue from the end of the D-helix. After Tyr-165, the last 26 amino acids remained unaccounted for crystallographically in all 144 subunits, and thus mutant C termini were longer than represented by Fig. 2*B*. We observed remarkable disruption and var-

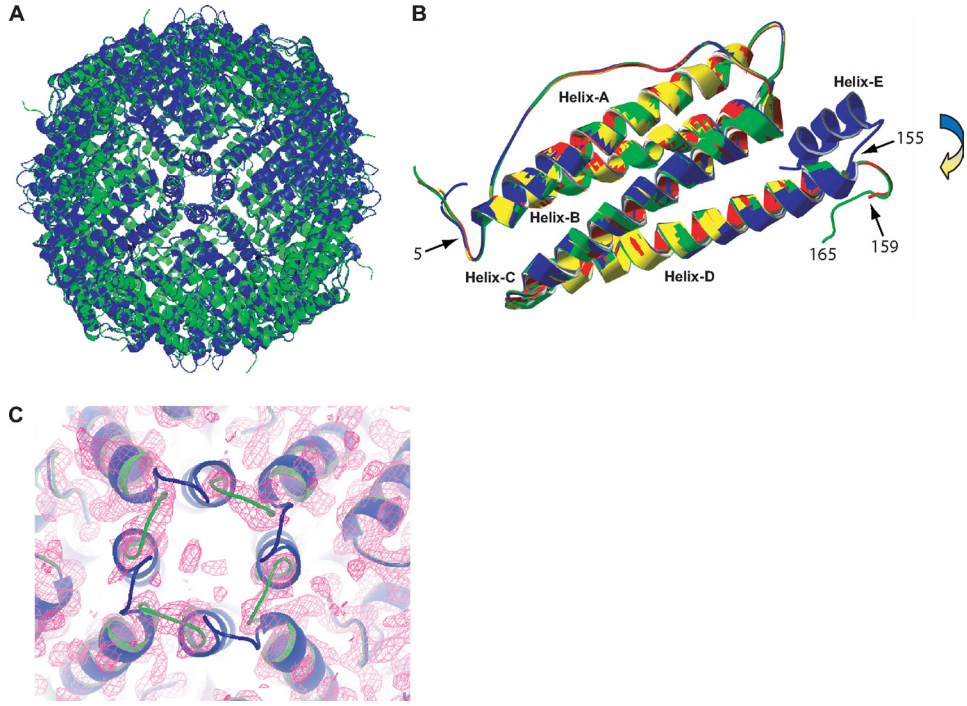

FIGURE 2. **Ribbon representations of WT- and MT-FTL homopolymer crystallographic structures.** *A,* overlay of the complete ferritin homopolymeric (24-subunit) structures of both WT- (*blue*) and MT-FTL (*green*) viewed down one of the 4-fold axes. *B,* overlay of the subunit structure of WT- (*blue*) and MT-FTL with different lengths of ordered C-terminal residues (*yellow,* Leu-155; *red,* Glu-159; *green,* Tyr-165), as observed crystallographically. The E-helix is missing in the mutant, and conformational differences between WT- and MT-FTL reach back to the D-helix (residue Leu-155), as detailed in the text. An additional 26 amino acids extend from Tyr-165, but were not observed in the electron density map and are not represented here. *C,* example of the omit σ_A-weighted $2F_o - F_c$ electron density contoured at one standard deviation surrounding one of the 4-fold axes in the mutant ferritin structure. The WT- (*blue*) and MT-FTL (*green*) structures are represented using a ribbon diagram for better clarity to view the changes in direction of the polypeptide chain in this region. *A* and *B* were produced using SPDB-Viewer and rendered with Pov-Ray. *C* was produced using PyMol for Windows (34).

iability at the 4-fold pores, which can be appreciated with a 10-Å thick slice through four of the six 4-fold pores of the wild type and mutant (Fig. 3, *A* and *B*). Whereas the pores are narrow and densely packed in the wild type, they were of variable structure and size in the mutant. Such disruption and variability were not generally evident throughout the mutant as made clear by a slice sampling the spherical structure perpendicular to the 3-fold axis (Fig. 3, *C* and *D*). This 4-fold pore variability is further accentuated by the differential positioning of the C-terminal polypeptides in different subunits of the mutant (Fig. 2*B*). As a consequence of the structural changes, the hydrophobic pores normally formed by the tight association of four E-helices around each 4-fold symmetry axis in the WT-FTL homopolymer were totally disrupted in the mutant.

From a crystallographic point of view, the lack of a single stable conformation at the C terminus gives the appearance of increased size pores surrounding the 4-fold axes in the structure (Figs. 2 and 3). However, because the C termini are present in the mutant protein, a more accurate view of the 4-fold pores would be an assembly of conformational states that are rapidly exchanging and ultimately lead to a leaky and unstable pore structure. With the absence of interpretable electron density data after Leu-155, there were subunits with 36 unaccounted for C-terminal residues, which could, if extended, be over 125 Å in length. The C-terminal residues when pointed outwards could extend significantly into solution and when pointed inwards could reach any point within the shell interior, *i.e.* the nucleation sites (or ferroxidase sites in the heteropolymer).

Deletion of the Mutant C-terminal Sequence Prevented Iron Loading-induced Precipitation—To determine whether protrusion of the MT-FTL C terminus above the protein shell had a role in solubility (28) or iron-induced precipitation, we compared the iron loading of apoferritin homopolymers of WT-, MT-, and TRUN-FTL. TRUN-FTL, a truncated form of FTL (p.S167X) with all mutated residues removed, assembled as an apoprotein homopolymer (24-mer), as verified by gel electrophoresis. Each homopolymer was incubated aerobically with increasing amounts of iron up to a maximum loading ratio of 4000:1 iron:homopolymer (24-mer) (Fig. 4). In contrast to MT-FTL homopolymers, which began to precipitate around 1500:1 (18), both the WT- and TRUN-FTL homopolymers remained in solution up to a 4000:1 ratio. Thus, removal of the mutant portion of the C terminus prevented iron-induced precipitation.

Mutant Homopolymers Had Decreased Initial Iron Incorporation Versus WT-FTL—To determine early alterations in iron incorporation, we measured the increase in absorbance at 310 nm over the first few minutes after aerobically mixing ferrous iron with apoferritin (Fig. 5). The rate of amber color development for MT-FTL ferritin was substantially less than that of the WT-FTL, and at 500 s, the total absorbance of the mutant was only ~20% of the wild type. An absorbance increase at 310 nm is routinely interpreted as incorporation/nucleation of iron within the ferritin shell, although it contains a hydrolysis component (29). The absorbance increase due to mixing ferrous iron with buffer alone was relatively minor and was included in the figure for comparison. Thus, MT-FTL showed pronounced alteration of iron handling through both initial uptake rate and cumulative iron incorporation inside the shell when examined over the first few minutes after mixing.

Mutant Homopolymers Did Not Incorporate Iron in the Presence of WT-FTL—We performed a modified assay in which both ferritin apoproteins were in the same solution competing for the incorporation of added iron (in a ratio of 1000:1 iron: homopolymer) with a 30-min incubation time (Fig. 6). When in separate solutions, both WT- and MT-FTL homopolymers had significant ability to incorporate iron (iron stain panel), but when in competition, there was complete absence of iron incorporation by MT-FTL. It should be noted that this absence is not due to iron-induced precipitation of MT-FTL in that no pellet

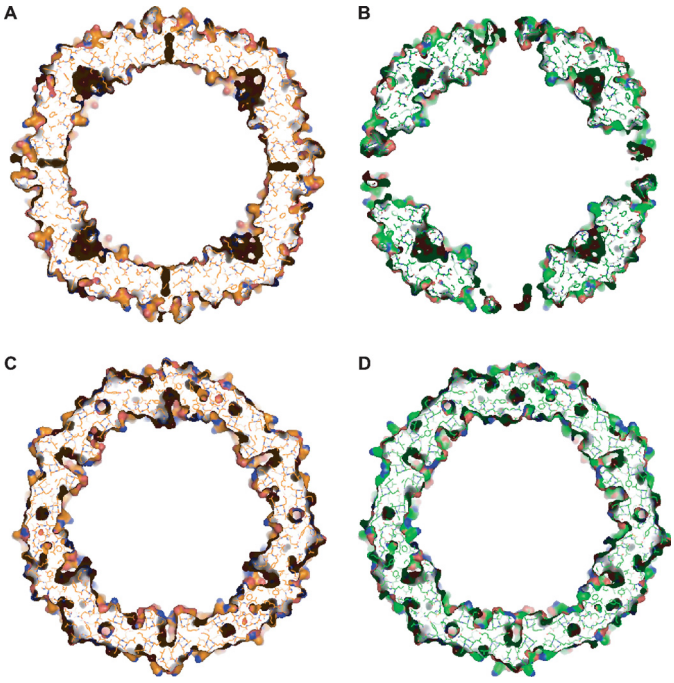

FIGURE 3. **Cross-sectional representations of WT- (*A* and *C*) and MT-FTL (*B* and *D*) crystallographic structures.** Each view represents a 10-Å thick slice through the middle of the 24-subunit assembly. *A* and *B* have the local 4-fold axes running horizontally and vertically and the local 2-fold axes running diagonally. *C* and *D* is a view down one of the 3-fold axes. Large but variable structural disruption is found along the 4-fold axes of the pores of the mutant but not the wild type. The C termini extended from Tyr-165 were not observed in the electron density map and are not represented here. *A–D* were produced using PyMol for Windows (34).

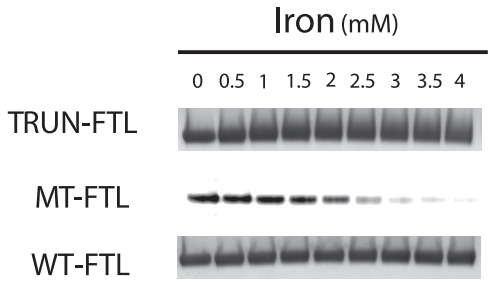

FIGURE 4. **Iron loading-induced precipitation of MT-FTL homopolymers.** Ferrous ammonium sulfate was added to WT-, TRUN-, and MT-FTL apoferritin homopolymers separately in 0.1 M Hepes, pH 7.0, and incubated for 2 h at 24 °C. Iron concentrations ranged from 0.0 to 4.0 mM with homopolymer fixed at 1 μM. Samples were centrifuged for 15 min at 10,000 × *g*, and soluble fractions were loaded onto native gels (3–8%) and stained with Coomassie Blue. With increasing iron concentration, MT-FTL homopolymers started to precipitate, whereas WT- and TRUN-FTL remained in solution.

was found in the centrifugation step for either FTL homopolymers (not shown). These results highlight the importance of direct iron mishandling by mutant ferritin without the effects of the iron-induced precipitation.

DISCUSSION

Here we report the x-ray crystallographic structure and functional studies of human ferritin homopolymers assembled from a mutant light chain variant (p.Phe167SerfsX26) that causes the neurodegenerative disease HF. Only recently have detailed crystallographic structures of human WT-FTL homopolymer become available (16), and herein is described the first structure

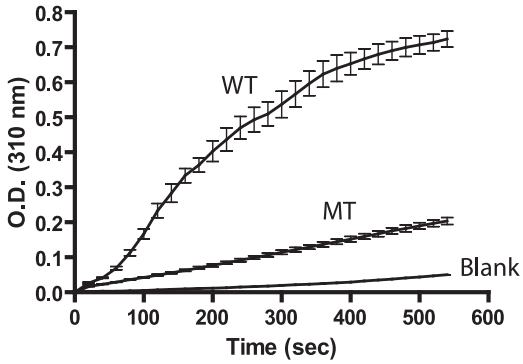

FIGURE 5. **Progression plots for iron incorporation into WT- and MT-FTL homopolymers.** Ferrous ammonium sulfate was mixed with either WT- or MT-FTL apoferritins separately in 0.1 M Hepes, pH 7.0, and iron incorporation/nucleation was monitored at 24 °C by the increase in absorbance at 310 nm. Iron concentration was 1 mM, and homopolymer was 1 μM. Plots show the mean ± S.E. as *error bars* of triplicate experiments. Iron incorporation was substantially reduced in the mutant homopolymers. The *blank* monitors iron hydrolysis in the absence of protein.

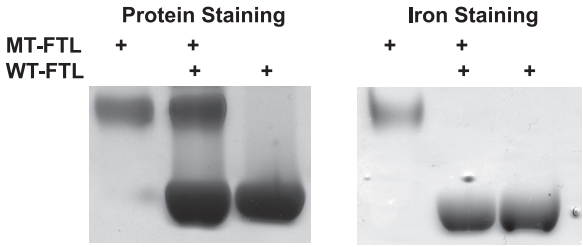

FIGURE 6. **Competition between WT- and MT-FTL homopolymers for iron incorporation.** WT- and MT-FTL apoferritins alone or mixed together in equimolar amounts (WT-FTL + MT-FTL) were incubated with ferrous ammonium sulfate in 0.1 M Hepes, pH 7.0, for 30 min at 24 °C. Iron concentration was 0.1 mM, and homopolymer was 0.1 μM. After centrifugation, samples were separated by electrophoresis in native gels (3–8%). Gels were stained with Coomassie Blue (*Protein Staining*) and Prussian blue (*Iron Staining*). No iron incorporation was found for the mutant when it was in direct competition with the wild type.

of one of six C-terminal insertional mutations in the FTL polypeptide associated with this disease.

MT-FTL subunits formed a spherical shell that was overall very similar to the wild type (30). Internal glutamic acid residues that form the iron nucleation site were visible and available for metal coordination. The 3-fold pores were basically the same. The main difference in structure between WT- and MT-FTL homopolymers was the lack of E-helices, which have a stabilizing influence on the 24-mer structure through intersubunit interactions among trans- and adjacent pairs of E-helices, as well as through intra-subunit interactions back to their respective subunits (31). The loss of E-helices and the presence of substantial amounts of disorder in the C terminus of the MT-FTL polypeptides lead to a significant disruption of the 4-fold axes pores. Interestingly, the mutation caused a conformational difference reaching back to the amino acid immediately after the end of the D-helix (Leu-155) even though the first mutated amino acid occurred at position 167 (F167S).

Although only a 10% difference in iron incorporation was observed over 2 h of iron loading (18), when iron incorporation into soluble ferritin was examined over a short time interval and with direct competition between the wild type and mutant as might be found in HF patients, MT-FTL homopolymers showed ~80% decrease in iron incorporation for over the first

500 s of the assay, and only the wild type incorporated iron when both mutant and wild type ferritin were together in solution. We suggest that iron mineral may begin to attach to the interior of the shell or iron may start to aggregate in combination with some portion of mutant C-terminal polypeptides to block mineral exit through the disordered 4-fold pores, with the result of some net iron accumulating over time. These data reveal a substantial problem with iron storage by soluble mutant ferritin that may be associated with the observed large disruption of the 4-fold pore, pointing toward the complexity of the ferritin portion of the overall iron management process with respect to HF and to the need for further study using animal models to complement *in vitro* work (32, 33).

Based on limited proteolysis and iron chelation data, we previously proposed that disordered C-terminal polypeptides in the mutant caused iron loading-induced precipitation of ferritin through iron bridging (18). The finding that truncation of the mutant C terminus prevented iron-induced precipitation further supports the notion that the C terminus of MT-FTL is an essential structural component of an exterior iron-binding site, which leads to *in vitro* precipitation and perhaps to inclusion body formation in HF. The disordered MT-FTL C terminus contains several ligands that can bind iron under appropriate conditions as follows: the terminal carboxylate, the glutamates, the tyrosinate, and perhaps even the serine and threonine hydroxyls and peptide backbone groups. Iron bridging and aggregation do not seem to involve covalent cross-linking via oxidation because we have not observed high molecular weight aggregates on SDS-PAGE from inclusion bodies isolated from patients with HF nor from transgenic mice (2, 32, 33) under nonreducing conditions. Furthermore, ferritin aggregates from transgenic mice and from recombinant MT-FTL were resolubilized using iron chelators *in vivo* and *in vitro* (18).

In conclusion, we have demonstrated the following: (i) substantial disruption and variability of the 4-fold pores in mutant FTL homopolymers through E-helix unraveling with little or no other change in 24-mer structure, and (ii) iron mishandling by soluble mutant FTL homopolymers. These results are consistent with the deregulation of cellular iron metabolism (ferritin loss of function) and overproduction of ferritin polypeptides (a positive feedback loop) observed in HF (8, 32, 33). Excess iron and ferritin would trigger the formation of ferritin aggregates, which may physically interfere with normal cellular functions (gain of a toxic function). It is hoped that these molecular level insights into the pathogenesis of HF will help in the development of therapies that may be able to either slow or halt its progression.

Acknowledgments—We thank the staff at 19-ID, especially Marianne Cuff, Norma Duke, and Steve Ginell. Argonne is operated by University of Chicago Argonne, LLC, for the United States Department of Energy, Office of Biological and Environmental Research under Contract DE-AC02-06CH11357.

REFERENCES

1. Curtis, A. R., Fey, C., Morris, C. M., Bindoff, L. A., Ince, P. G., Chinnery, P. F., Coulthard, A., Jackson, M. J., Jackson, A. P., McHale, D. P., Hay, D., Barker, W. A., Markham, A. F., Bates, D., Curtis, A., and Burn, J. (2001) *Nat. Genet.* **28,** 350–354
2. Vidal, R., Ghetti, B., Takao, M., Brefel-Courbon, C., Uro-Coste, E., Glazier, B. S., Siani, V., Benson, M. D., Calvas, P., Miravalle, L., Rascol, O., and Delisle, M. B. (2004) *J. Neuropathol. Exp. Neurol.* **63,** 363–380
3. Mancuso, M., Davidzon, G., Kurlan, R. M., Tawil, R., Bonilla, E., Di Mauro, S., and Powers, J. M. (2005) *J. Neuropathol. Exp. Neurol.* **64,** 280–294
4. Ohta, E., Nagasaka, T., Shindo, K., Toma, S., Nagasaka, K., Ohta, K., and Shiozawa, Z. (2008) *Neurology* **70,** 1493–1494
5. Kubota, A., Hida, A., Ichikawa, Y., Momose, Y., Goto, J., Igeta, Y., Hashida, H., Yoshida, K., Ikeda, S., Kanazawa, I., and Tsuji, S. (2009) *Mov. Disord.* **24,** 441–445
6. Devos, D., Tchofo, P. J., Vuillaume, I., Destée, A., Batey, S., Burn, J., and Chinnery, P. F. (2009) *Brain* **132,** e109
7. Vidal, R., Delisle, M. B., Rascol, O., and Ghetti, B. (2003) *J. Neurol. Sci.* **207,** 110–111
8. Vidal, R., Delisle, M. B., and Ghetti, B. (2004) *J. Neuropathol. Exp. Neurol.* **63,** 787–800
9. Maciel, P., Cruz, V. T., Constante, M., Iniesta, I., Costa, M. C., Gallati, S., Sousa, N., Sequeiros, J., Coutinho, P., and Santos, M. M. (2005) *Neurology* **65,** 603–605
10. Theil, E. C., Matzapetakis, M., and Liu, X. (2006) *J. Biol. Inorg. Chem.* **11,** 803–810
11. Harrison, P. M., and Arosio, P. (1996) *Biochim. Biophys. Acta* **1275,** 161–203
12. Theil, E. C. (2003) *J. Nutr.* **133,** 1549S–1553S
13. Ford, G. C., Harrison, P. M., Rice, D. W., Smith, J. M., Treffry, A., White, J. L., and Yariv, J. (1984) *Philos. Trans. R. Soc. Lond. B Biol. Sci.* **304,** 551–565
14. Harrison, P. M., Ford, G. C., Smith, J. M., and White, J. L. (1991) *Biol. Met.* **4,** 95–99
15. Hempstead, P. D., Yewdall, S. J., Fernie, A. R., Lawson, D. M., Artymiuk, P. J., Rice, D. W., Ford, G. C., and Harrison, P. M. (1997) *J. Mol. Biol.* **268,** 424–448
16. Wang, Z., Li, C., Ellenburg, M., Soistman, E., Ruble, J., Wright, B., Ho, J. X., and Carter, D. C. (2006) *Acta Crystallogr. D. Biol. Crystallogr.* **62,** 800–806
17. Takahashi, T., and Kuyucak, S. (2003) *Biophys. J.* **84,** 2256–2263
18. Baraibar, M. A., Barbeito, A. G., Muhoberac, B. B., and Vidal, R. (2008) *J. Biol. Chem.* **283,** 31679–31689
19. Levi, S., Luzzago, A., Cesareni, G., Cozzi, A., Franceschinelli, F., Albertini, A., and Arosio, P. (1988) *J. Biol. Chem.* **263,** 18086–18092
20. Fish, W. W. (1988) *Methods Enzymol.* **158,** 357–364
21. Navaza, J. (2001) *Acta Crystallogr. D Biol. Crystallogr.* **57,** 1367–1372
22. Brünger, A. T., Adams, P. D., Clore, G. M., DeLano, W. L., Gros, P., Grosse-Kunstleve, R. W., Jiang, J. S., Kuszewski, J., Nilges, M., Pannu, N. S., Read, R. J., Rice, L. M., Simonson, T., and Warren, G. L. (1998) *Acta Crystallogr. D Biol. Crystallogr.* **54,** 905–921
23. Emsley, P., and Cowtan, K. (2004) *Acta Crystallogr. D Biol. Crystallogr.* **60,** 2126–2132
24. Levi, S., Salfeld, J., Franceschinelli, F., Cozzi, A., Dorner, M. H., and Arosio, P. (1989) *Biochemistry* **28,** 5179–5184
25. Levi, S., Santambrogio, P., Cozzi, A., Rovida, E., Corsi, B., Tamborini, E., Spada, S., Albertini, A., and Arosio, P. (1994) *J. Mol. Biol.* **238,** 649–654
26. Santambrogio, P., Levi, S., Cozzi, A., Corsi, B., and Arosio, P. (1996) *Biochem. J.* **314,** 139–144
27. Levi, S., Yewdall, S. J., Harrison, P. M., Santambrogio, P., Cozzi, A., Rovida, E., Albertini, A., and Arosio, P. (1992) *Biochem. J.* **288,** 591–596
28. Ingrassia, R., Gerardi, G., Biasiotto, G., and Arosio, P. (2006) *J. Biochem.* **139,** 881–885
29. Baes, C. F., and Mesmer, R. E. (1976) *The Hydrolysis of Cations,* pp. 489, John Wiley & Sons, New York

30. Granier, T., Gallois, B., Langlois d'Estaintot, B., Dautant, A., Chevalier, J. M., Mellado, J. M., Beaumont, C., Santambrogio, P., Arosio, P., and Precigoux, G. (2001) *Acta Crystallogr. D Biol. Crystallogr.* **57,** 1491–1497
31. Crichton, R. R., and Pierre, J. L. (2001) *Biometals* **14,** 99–112
32. Vidal, R., Miravalle, L., Gao, X., Barbeito, A. G., Baraibar, M. A., Hekmatyar, S. K., Widel, M., Bansal, N., Delisle, M. B., and Ghetti, B. (2008) *J. Neurosci.* **28,** 60–67
33. Barbeito, A. G., Garringer, H. J., Baraibar, M. A., Gao, X., Arredondo, M., Núñez, M. T., Smith, M. A., Ghetti, B., and Vidal, R., (2009) *J. Neurochem.* **109,** 1067–1078
34. DeLano, W. L. (2002) *The PyMOL Molecular Graphics System,* DeLano Scientific, San Carlos, CA